

Synthesis and thermal expansion of chalcogenide MAX phase Hf₂SeC

Xudong Wang ^{a,b,#}, Ke Chen ^{a,c,#,*}, Erxiao Wu ^a, Yiming Zhang ^{a,c}, Haoming Ding ^a,
Nianxiang Qiu ^{a,c}, Yujie Song ^{a,c}, Shiyu Du ^{a,c}, Zhifang Chai ^{a,c}, Qing Huang ^{a,c,*}

^a Engineering Laboratory of Advanced Energy Materials, Ningbo Institute of Materials Technology and Engineering, Chinese Academy of Sciences, Ningbo 315201, China.

^b School of Materials Science and Engineering, Shanghai University, Shanghai 200444, China

^c Qianwan Institute of CNiTECH, Ningbo 315336, China.

[#] These authors contributed equally to this work.

^{*} Corresponding authors.

E-mail addresses: chenke@nimte.ac.cn (Ke Chen), huangqing@nimte.ac.cn (Qing Huang).

Abstract

Thermal expansion of MAX phases along different directions tended to be different because of the anisotropy of hexagonal crystals. Herein, a new Hf₂SeC phase was synthesized and confirmed to be relatively isotropic, whose coefficients of thermal expansion (CTEs) were determined to be 9.73 μK⁻¹ and 10.18 μK⁻¹ along *a* and *c* directions. The strong M-S bond endowed Hf₂SC and Zr₂SC lower CTEs than Hf₂SeC and Zr₂SeC. A good relationship between the thermal expansion anisotropy and the ratio of elastic stiffness constant *c*₁₁ and *c*₃₃ was established. This straightforward approximation could be used to roughly predict the thermal expansion anisotropy of MAX phases.

Key words: MAX phase, Hf₂SeC, thermal expansion, anisotropy

1. Introduction

MAX phases emerged in 1960s, are a large family of layered ternary compounds [1]. These early transition-metal carbides and nitrides have a general chemical formula $M_{n+1}AX_n$; wherein M is an early transition metal, A mainly comes from A-group element, X is carbon and/or nitrogen, $n = 1 - 3$ [1, 2]. Due to the combining properties of both metals and ceramics, MAX phases have good high-temperature stability, good damage tolerant, high thermal conductivity, as well as excellent resistance to oxidation and corrosion [1-4]. Most of the physical and chemical properties of MAX phases are anisotropic because of the layered, hexagonal crystal structure, whose edge-sharing covalent M_6X octahedrons are interleaved by close-packed metallic A layers [1, 2]. However, anisotropic crystal sometimes is harmful to the applications of MAX phases, especially in extreme environments including high temperature and intense irradiation fields. For instance, the grain boundary cracking induced by energetic heavy ion (5.8 MeV Ni) could be manifested by the anisotropic swelling [5]. Hence, the relatively isotropic Ti_3SiC_2 with similar elastic modulus along a and c directions exhibited better irradiation damage tolerant than aluminum-based MAX phases (Ti_3AlC_2 and Ti_2AlC) [5, 6].

Ti_2SC is compact in crystal structure, having a much smaller c/a value and stronger M-A bond compared with the other 211-MAX phases [7, 8]. Hence, the thermal expansion anisotropy of Ti_2SC is relatively low, whose coefficients of thermal expansions (CTE) along a and c directions were $8.6 \mu K^{-1}$ and $8.7 \mu K^{-1}$ [6, 9]. The high bond strength of M-A can also be found in the newly synthesized chalcogenide MAX phase, Zr_2SeC . The calculation of density of states confirms the strong interaction between outer electrons of Zr and that of Se [10, 11]. Herein, Hf_2SeC was successfully prepared to further explore the thermal expansion anisotropy of this series of new Se-MAX phases. The expanded crystal parameters of Hf_2SeC powders were measured and calculated by high-temperature X-ray diffraction and subsequent Rietveld refinement from ambient temperature to 600 °C using Hf_2SC , Zr_2SeC , and Zr_2SC as comparative analyses. The elastic stiffness constants were calculated to plot the influence of A-site elements on the thermal expansion anisotropy of these chalcogenide MAX phases.

2. Experimental

2.1 Synthesis details

To begin with, considering the low melting and boiling points of selenium, the hafnium diselenide was synthesized using commercially hafnium (99.9% purity, 400 nm, Beijing Xingrongyuan Technology Co., Ltd. China) and selenium (99.99% purity, 200 mesh, Aladdin) powders in a sealed quartz tube at 950°C for 24 hours [12]. Hf_2SeC was synthesized using the mixture of hafnium, self-made hafnium diselenide and carbon (99.9% purity, 400 nm, Macklin, China) powders with a ratio of 3:1.05:1.9. The ground powder mixture was pre-pressed in a graphite die with $\Phi 20$ mm. The reaction process was performed in a Pulse-Electric-Current-Aided sintering device (HPD 25/3, FCT Group, Germany) at the temperature of 1600 °C for 10 min with a maximum uniaxial pressure of 48 MPa under Ar atmosphere. In whole reaction process, the initial heating rate was 50 °C/min in the temperature range of 450-1100°C and reduced to 25 °C/min after 1100°C, and the cooling rate was 50°C/min in the temperature range of 1600-450°C.

In addition, Hf_2SC , Zr_2SeC and Zr_2SC , were also prepared for comparative analyses. The precursors HfS_2 , ZrSe_2 and ZrS_2 were synthesized at 950°C, 900°C and 950°C in the same method [12, 13]. It was worth reminding that the raw materials sulfur (99.99% purity, 300mesh, General Research Institute for Nonferrous Metals, China) and zirconium (99.5% purity, 400mesh, Targets Research Center of General Research Institute for Nonferrous Metals, China) were commercially available powders. The Hf_2SC , Zr_2SeC and Zr_2SC phases were *in-situ* synthesized using self-made transition-metal dichalcogenide, commercially metal and carbon powders with a stoichiometric ratio of 1.05:2.9:1.9, 1.05:3:1.9 [10] and 1:3:2 [14]. The reaction process was the same as the method for Hf_2SeC except the sintering temperature of 1500°C. Finally, the as-obtained bulks were ground with 1 μm -diamond grinding paste for subsequent characterization.

2.2 Materials characterization

The as-synthesized powders were examined and analyzed using X-ray diffractometer

(XRD; Bruker AXS D8 Advance, Germany) with Cu K α ray under an operating power of 1600 W (40 mA and 40 kV) at a step scan of 0.02 °/2 θ and a step time of 0.2s. The lattice parameters and phase composition of the synthesized phases were determined by the Rietveld method using the software of *TOPAS-Academic v6*. The fracture micromorphology and chemical composition of the specimens were studied by the scanning electron microscope (SEM; Hitachi Regulus 8230, Japan) equipped with energy dispersive spectroscopy (EDS). Furthermore, thin foils were prepared by focused ion beam (FIB; Thermo scientific Helios-G4-CX, USA) technique and were observed furtherly by a transmission electron microscope (TEM; Spectra 300, USA).

Coefficients of linear expansion (CTEs) in the *a* and *c* directions of the as-synthesized MAX phases powders were studied by the high-temperature XRD diffractometer (XRD; Bruker D8 Advance, Germany) with a furnace in vacuum (10⁻² mbar). The XRD data were taken from 5°–70° in steps of 0.02° with hold times of 0.2 s/step from room temperature to 873K. The heating rate was 60 °C/min with a 10 min holding time prior to each scan. Rietveld analysis was performed on the high-temperature XRD patterns using the *TOPAS-Academic v6* to calculate the expanded lattice parameters.

2.3 Calculation Details

The calculations were performed by the *Vienna Ab initio Computing Software Package* [15, 16], and the projector-augmented wave method [17] with an energy cutoff of 500 eV. The Perdew–Burke–Ernzerhof (PBE) version of the generalized gradient approximation (GGA) [18] was used for the exchange and correlation functionals. In order to keep the forces on each atom of the crystal structure model less than 1.0×10^{-4} eV/Å and the total energy converged at 1.0×10^{-8} eV/cell, the crystal structure was relaxed according to the conjugate gradient scheme [19].

The Brillouin Zones (BZs) of MAX phases configurations were described with a Γ -centered *k*-point mesh of $12 \times 12 \times 4$. The density of states was plotted by the Gaussian smearing with a broadening of 0.01 eV. The bulk states were optimized through relaxing all the volume, lattice parameters, and atomic positions. For crystals with hexagonal

symmetry, elastic stiffness constants are calculated based on the stress–strain relationship [20].

3. Results and discussion

The as-synthesized bulks were characterized using X-ray diffraction from 5 ° to 70 ° (**Figure 1(a)**). Rietveld fitting results (reliability factors $R_{wp} = 8.29\%$) showed that the crystal structure of predominant phase belonged to hexagonal structure ($P6_3/mmc$, No. 194), which was the characteristic structure of MAX phase (**the inset in Figure 1(a)**) [1]. The determined composition was 95.2 wt. % Hf_2SeC with small amount of residual HfO_2 . The respective coordinates of component elements in this chalcogenide MAX phase were Hf ($1/3, 2/3, 0.0953$), Se ($1/3, 2/3, 3/4$), and C ($0, 0, 0$), and fitting lattice parameters were $a = 0.3422$ nm and $c = 1.2391$ nm, respectively. This lattice parameter was in good agreement with the analysis of TEM. Wherein, the value of a and c were identified to be 0.3387 nm and 1.2327 nm according to the selected area electron diffraction (SAED) (**the inset in Figure 1(c)**). The first-principles calculations were also performed to verify the formation of Hf_2SeC MAX phase. The calculated lattice parameters were $a = 0.3436$ nm and $c = 1.2452$, and z position in coordinate of Hf atom was 0.0943. The fracture morphology and composition of the as-synthesized products were characterized by SEM (**Figure 1(b)**). The hexagonal grains with size of about 1 μm were observed indicating the intergranular fracture of the as-synthesized Hf_2SeC bulk. EDS results showed that the composition of the main particles contained Hf, Se and C. The ratio of Hf to Se was close to 2: 1 (**Table S1, Figure S1**), indicating the formation of Hf_2SeC . The crystal structure and atom arrangements within the Hf_2SeC along the $[11\bar{2}0]$ zone axis was visually observed via advanced atom-resolved high-angle annular dark-field (HAADF) technique (**Figure 1(c)**). The HAADF image is related to atomic number contrast, *i.e.*, the larger the atomic number is, the brighter the atom will be [21]. It was easily to distinguish that two lines of bigger and brighter dots (Hf, also marked in crimson) interleaved with one lines of smaller and dimmer dots (Se, also marked in cyan) (**Figure 1(d-f)**). This mirrored zig-zag arrangement was the characteristic of 211 MAX phase [1, 3].

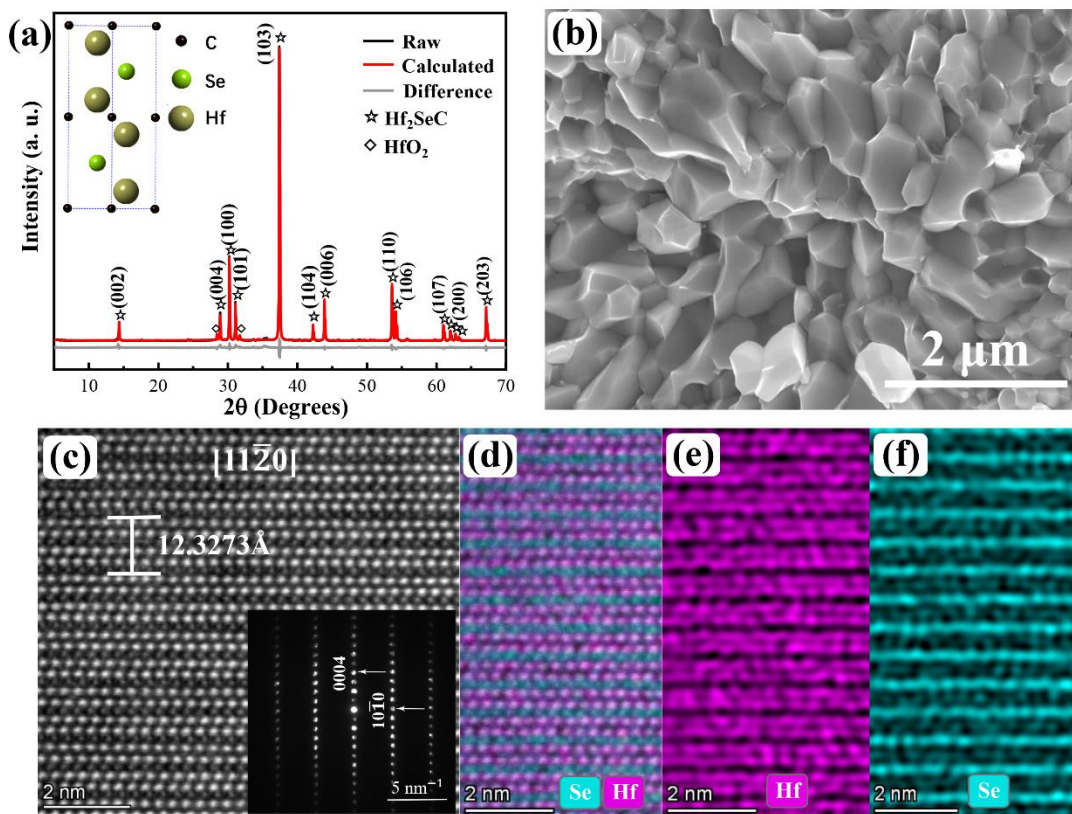


Figure 1. (a) XRD patterns of as-synthesized Hf_2SeC . (b) SEM image of the Hf_2SeC . (c) High-resolution image of the Hf_2SeC showing atomic positions along $[11\bar{2}0]$ direction, the inset was corresponding selected area electron diffraction. (d-f) Atom-resolved EDS mapping images.

Thermal expansion is one of the important thermal properties for the high-temperature applications, which is induced by the anharmonic vibration of atoms in temperature field. Herein, the expanded lattice parameters of as-synthesized Hf_2SeC powders were measured by high-temperature X-ray diffraction from ambient temperature to 873 K (**Figure 2(a-c)**). It was clearly that the Hf_2SeC peaks noticeably shifted to the left with increasing temperature, which indicated the expansion of lattice structure. Among them, the evolutions of (103) peaks and (002) peaks were the typical to show the thermal expansion of MAX phases along a and c directions. The expanded lattice parameters were then determined by Rietveld refinements using *TOPAS-Academic v6*. The evolutions of refined lattice parameters were linearly fitted using Zr_2SeC , Hf_2SC , and Zr_2SC as comparative analyses (**Figure 2(d-e)**, **Figure S2** and

Table S2). The coefficients of thermal expansion (CTEs) along a and c directions (α_a and α_c) were calculated as follows [22]:

$$\alpha_a = \frac{d(a(T))}{a_0 dT} \text{ and } \alpha_c = \frac{d(c(T))}{c_0 dT} \quad (1)$$

Where, $\frac{d(a(T))}{dT}$ and $\frac{d(c(T))}{dT}$ are the slopes of fitted linear functions of $a(T)$ and $c(T)$. a_0 and c_0 are the lattice parameters at ambient temperature. The mean CTE (α_{av}) was then calculated as follows [22]:

$$\alpha_{av} = \frac{2\alpha_a + \alpha_c}{3} \quad (2)$$

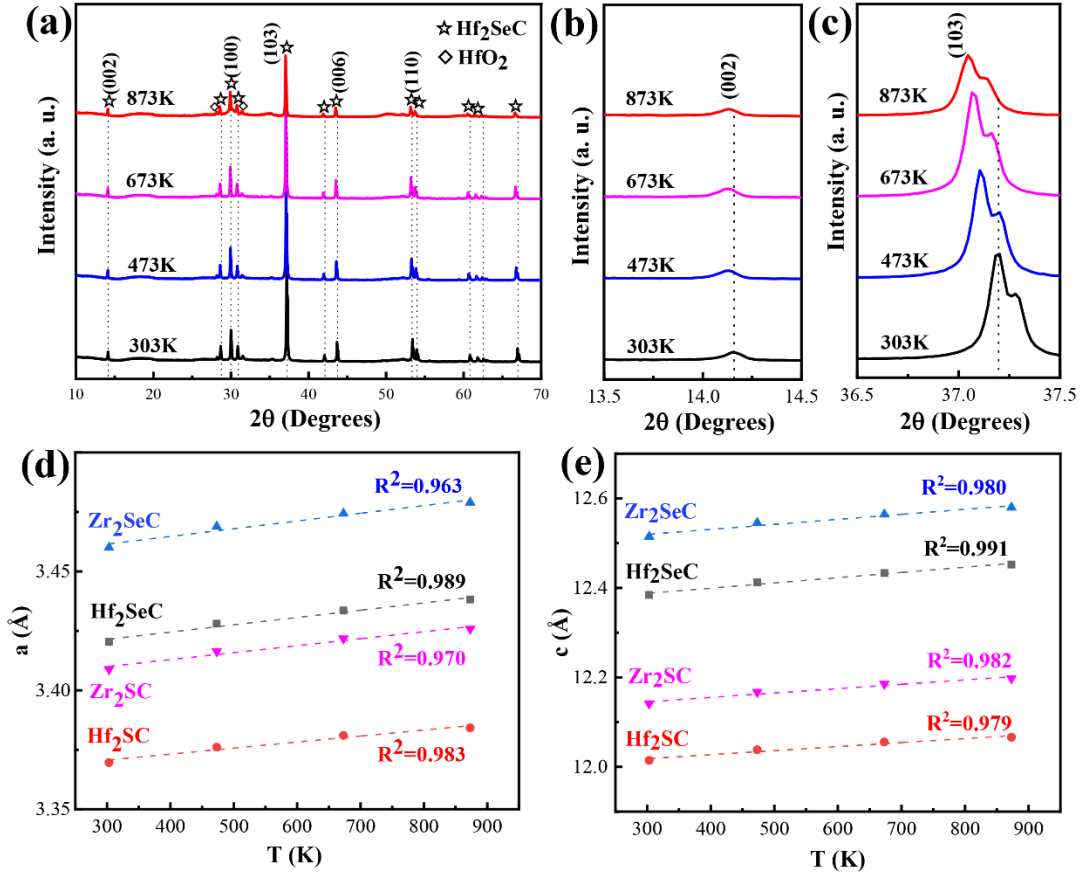


Figure 2. (a-c) High-temperature XRD patterns of Hf₂SeC. (d-e) Temperature dependence of the lattice parameters a and c for Hf₂SeC, Hf₂SC, Zr₂SeC and Zr₂SC.

Herein, α_a , α_c , and α_{av} of Hf₂SeC were given to be 9.73 μK^{-1} , 10.18 μK^{-1} , and 9.88 μK^{-1} , respectively. And CTEs of Zr₂SeC, Hf₂SC, and Zr₂SC were shown in **Table 1**. Interestingly, the CTEs of Se-MAX phases were larger than those of S-MAX phases,

which indicated that the A-group elements played an important role in the thermal expansion of MAX phase. This discrepancy could be tentatively explained by the regulation of M–A bond length in these nanolaminated carbides. Compared with sulfur, selenium is larger in atomic size and has a smaller electronegativity. The occupation of Se in A site lengthened the M-A bond length of M-S, which was verified by first-principles calculation. Wherein, the bond length for Hf-Se and Zr-Se were 2.774 Å and 2.800 Å, while the bond length for Hf-S, and Zr-S were 2.662 Å and 2.691 Å, respectively (**Table S3**). This weakened bonding energy of Zr-Se than that of Zr-S was also confirmed by the analysis of density of states in the previous works [10, 11]. The soft crystal structure benefited the amplitude of vibration as reflected a high thermal expansion in Hf₂SeC and Zr₂SeC.

Table 1. Coefficients of thermal expansion and thermal expansion anisotropy for Hf₂SeC, Hf₂SC, Zr₂SeC and Zr₂SC.

Compound	α_a (μK^{-1})	α_c (μK^{-1})	α_c/α_a	α_{av} (μK^{-1})
Hf ₂ SeC ^a	9.73	10.18	1.05	9.88
Hf ₂ SC ^a	7.51	7.49	1.00	7.50
Zr ₂ SeC ^a	9.36	8.94	0.95	9.22
Zr ₂ SC ^a	8.61	8.04	0.93	8.42
Ti ₂ SC ^b	8.61	8.72	1.01	8.65

^a Present work

^b Reference [6]

Table 2. The Elastic stiffness constants and subsequently calculated Grüneisen parameters for Hf₂SeC, Hf₂SC, Zr₂SeC and Zr₂SC.

Compound	c_{11} (GPa)	c_{12} (GPa)	c_{13} (GPa)	c_{33} (GPa)	c_{44} (GPa)	γ_c/γ_a
Hf ₂ SeC ^a	308	93	105	314	135	1.05
Hf ₂ SC ^a	330	100	118	345	150	1.06
Zr ₂ SeC ^a	275	82	92	289	125	1.03
Zr ₂ SC ^a	295	91	100	318	135	1.04
Ti ₂ SC ^b	339	90	100	354	162	1.05

^a Present work

^b Reference [6]

It was noteworthy that the α_c and α_a of Hf₂SeC, Hf₂SC, Zr₂SeC, and Zr₂SC are almost the same (**Table 1**). The degree of anisotropy ratios for thermal expansion could be described as α_c/α_a . The values of α_c/α_a for these four chalcogenide MAX phases were close to 1 (*i.e.*, Hf₂SeC, Hf₂SC, Zr₂SeC, and Zr₂SC were 1.05, 1.00, 0.95, and 0.93 respectively), suggesting the isotropic expansion with the increasing temperature. This phenomenon is not too surprising since the bond stiffness of M-A and M-X associated with the anisotropy in thermal expansion are similar in the chalcogenide MAX phase [6, 11]. However, Ti₂AlC, as a common example of Al-MAX phase, had a very large difference between the bond stiffness of Ti-Al and Ti-C [24], whose value of α_c/α_a was 1.41 [8]. In order to further discuss the influence of chalcogenide A-site elements on the anisotropy in thermal expansion, these four values of α_c/α_a were plotted in the conclusion of previous work (**Figure 3(a)**) [6]. It was interesting that the anisotropy of α_c/α_a increased with the rising A-site group number of MAX phase, and fell down over the IVA group. The anisotropy points of as-synthesized chalcogenide MAX phases clustered near the line of $\alpha_c/\alpha_a = 1$. The phenomenon could be tentatively explained by the analysis of Grüneisen parameter, which quantified the anharmonic vibration of atoms [25]. In the hexagonal symmetry, the Grüneisen parameters along a and c directions (γ_a and γ_c) were calculated as follows [6, 26]:

$$\gamma_a = \frac{V_m}{C_v} [(c_{11} + c_{12})\alpha_a + c_{13}\alpha_c] \quad (3)$$

$$\gamma_c = \frac{V_m}{C_v} (2c_{13}\alpha_a + c_{33}\alpha_c) \quad (4)$$

Where, V_m is the molar volume. C_v is the molar specific heat at constant volume, which is $3NR$ assumed as the application of Dulong–Petit law (N is the number of atoms per unit cell and R is the ideal gas constant). c_{ij} is an elastic stiffness constant (five independent elastic stiffness constants c_{11} , c_{12} , c_{13} , c_{33} , and c_{44} for hexagonal symmetry). This derivation implied that the thermal expansion was mainly associated with the elastic stiffness constants. The anisotropy of thermal expansion could also be described using the ratio of γ_c to γ_a . The calculated values of γ_a and γ_c for Hf_2SeC , Hf_2SC , Zr_2SeC , and Zr_2SC were between 1 to 2, and the ratios of γ_c to γ_a were near 1, which indicated that the thermal expansion of these along a and c directions was almost the same in these chalcogenide MAX phases. For comparison, the largest thermal expansion anisotropy belonging to Nb_2AsC (**Figure 3(a)**). Scabarozzi et al simplified the linear correlation between thermal expansion anisotropy with the elastic stiffness constant c_{13} in 211-MAX phase. The anisotropy was concluded related to the bonding between the M–A elements [6]. Herein, the relationship between thermal expansion anisotropy and value of c_{11}/c_{33} was plotted to further discuss the influence of A-site elements on the thermal expansion anisotropy of these chalcogenide MAX phases. The thermal expansion of MAX phase tended to isotropy when the value of c_{11}/c_{33} was close to 1, since the c_{11} and c_{33} reflected the bonding strengths in the a and c directions of hexagonal crystals. This criterion was roughly effective for the most MAX phases concluded in **Figure 3(b)**. The as-synthesized chalcogenide MAX phases, Hf_2SeC , Hf_2SC , Zr_2SeC , and Zr_2SC , whose c_{11} was similar to c_{33} , had relatively isotropic thermal expansion. While Al-MAX phases, such as Ti_2AlC and Ti_3AlC_2 , were relatively anisotropic in thermal expansion due to the large difference of c_{11} and c_{33} . The thermal expansion anisotropy of Nb_2SnC , Nb_2AsC , V_2GeC , and V_2AsC were abnormally large. The reason probably resulted from the large values of c_{12} and c_{13} . Wherein, the differences between c_{12} or c_{13} and c_{11} or c_{33} were much larger than those of other MAX phases [6, 8, 27]. The above analyses means that the approximation is valid when the

elastic stiffness constants normal to the expanded plain can be neglected comparing to those in the plain. This straightforward approximation could be used to roughly predict the thermal expansion anisotropy of MAX phases.

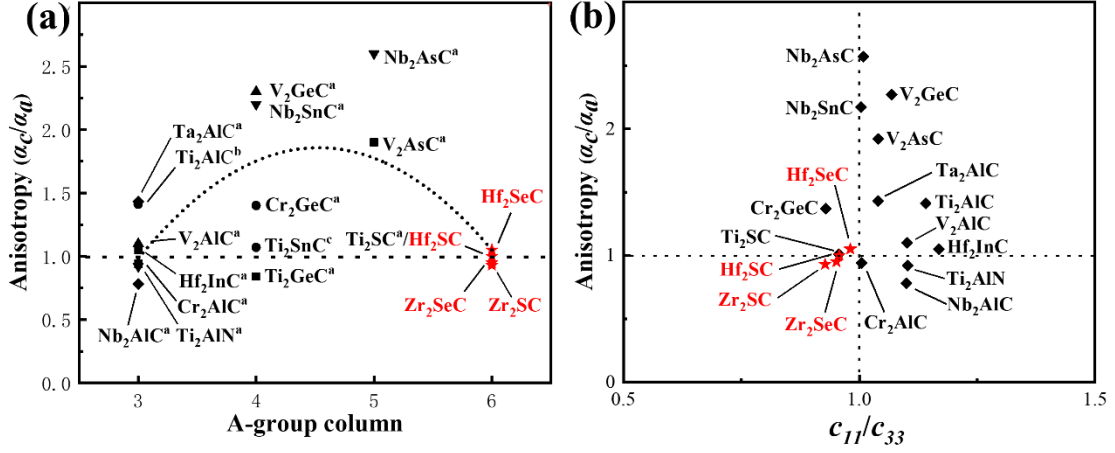


Figure 3. Thermal expansion properties of common MAX phases and the as-characterized four chalcogenide MAX phases were marked in red: **(a)** Anisotropy in thermal expansion vs A-group elements. **(b)** Anisotropy in thermal expansion vs elastic stiffness constant ratio of c_{11}/c_{33} .

^a Reference [6]

^b Reference [8]

^c Reference [27]

4. Conclusions

In summary, a new chalcogenide MAX phase Hf_2SeC was synthesized and characterized. The CTEs of Hf_2SeC along a and c directions were determined to be $9.73 \mu\text{K}^{-1}$, and $10.18 \mu\text{K}^{-1}$, respectively. Due to the stronger M-A bond, S-MAX phases (Hf_2SC and Zr_2SC) had lower CTEs than those of Se-MAX phases (Hf_2SeC and Zr_2SeC). These four chalcogenide MAX phases were relatively isotropic in thermal expansion, which agreed with the approximation of correction between anisotropy and c_{11}/c_{33} .

Declaration of Competing Interest

No potential conflict of interest was reported by the authors.

Acknowledgements

This study was financially supported by the National Natural Science Foundation of China (Grant No. 51902319), International Partnership Program of Chinese Academy of Sciences (Grant No. 174433KYSB20190019), Leading Innovative and Entrepreneur Team Introduction Program of Zhejiang (Grant No. 2019R01003), Ningbo Top-talent Team Program and Ningbo “3315 plan” (Grant No. 2018A-03-A).

Appendix A. Supplementary data

Supplementary material related to this article can be found, in the online version, at <https://doi.org/10.1016/j.jeurceramsoc.20xx.xx.xxx>.

References

- [1] Barsoum MW. The $M_{n+1}AX_n$ Phases: A New Class of Solids. *Prog Solid St Chem* 28(1-4) (2000) 201-281.
- [2] M. Sokol, V. Natsu, S. Kota, M.W. Barsoum, On the Chemical Diversity of the MAX Phases, *Trends Chem* 1(2) (2019) 210-223.
- [3] Wang CX, Yang TF, Tracy CL, et al. Disorder in $M_{n+1}AX_n$ phases at the atomic scale, *Nat Commun* 10 (2019) 622.
- [4] Z. Wang, J. Shuai, B. Xu, A. Wang, P. Ke, A high oxidation resistance Ti_2AlC coating on Zirloy substrates for loss-of-coolant accident conditions, *Ceram Int* 45(11) (2019) 13912-13922.
- [5] D.W. Clark, S.J. Zinkle, M.K. Patel, C.M. Parish, High temperature ion irradiation effects in MAX phase ceramics, *Acta Mater* 105 (2016) 130-146.
- [6] T.H. Scabarozi, S. Amini, O. Leaffer, A. Ganguly, S. Gupta, W. Tambussi, S. Clipper, I.J.E. Spanier, M.W. Barsoum, J.D. Hettinger, Thermal expansion of select $M_{n+1}AX_n$ (M = early transition metal, A = A group element, X = C or N) phases measured by high temperature x-ray diffraction and dilatometry, *J Appl Phys* 105(1)

(2009) 0021-8979.

- [7] K. Chen, Q. Ye, J. Zhou, L. Shen, J. Xue, Q. Huang, Synthesis of Ti_2SC Phase Using Iron Disulfide or Iron Sulfide Post-Treated with Acid, *J Am Ceram Soc* 98(4) (2015) 1074-1079.
- [8] M.W. Barsoum, M. Ali, T. El-Raghy, Processing and characterization of Ti_2AlC , Ti_2AlN , and $\text{Ti}_2\text{AlC}_{0.5}\text{N}_{0.5}$, *Metall Mater Trans A* 31(7) (2000) 1857-1865.
- [9] S.R. Kulkarni, M. Merlini, N. Phatak, S.K. Saxena, G. Artioli, S. Amini, M.W. Barsoum, Thermal expansion and stability of Ti_2SC in air and inert atmospheres, *J Alloy Compd* 469(1-2) (2009) 395-400.
- [10] K. Chen, X. Bai, X. Mu, P. Yan, N. Qiu, Y. Li, J. Zhou, Y. Song, Y. Zhang, S. Du, Z. Chai, Q. Huang, MAX phase Zr_2SeC and its thermal conduction behavior, *J Eur Ceram Soc* 41(8) (2021) 4447-4451.
- [11] M.A. Ali, M.W. Qureshi, Newly synthesized MAX phase Zr_2SeC : DFT insights into physical properties towards possible applications, *Rsc Adv* 11(28) (2021) 16892-16905.
- [12] M.J. Mleczko, C.F. Zhang, H.R. Lee, H.H. Kuo, B. Magyari-Kope, R.G. Moore, Z.X. Shen, I.R. Fisher, Y. Nishi, E. Pop, HfSe_2 and ZrSe_2 : Two-dimensional semiconductors with native high-kappa oxides, *Sci Adv* 3(8) (2017) 1-9.
- [13] B.G. Yacobi, F.W. Boswell, J.M. Corbett, Intercalation-Induced Shift of the Absorption-Edge in ZrS_2 and HfS_2 , *J Phys C Solid State* 12(11) (1979) 2189-2196.
- [14] M. Opeka, J. Zaykoski, I. Talmy, S. Causey, Synthesis and characterization of Zr_2SC ceramics, *Mat Sci Eng a-Struct* 528(4-5) (2011) 1994-2001.
- [15] G. Kresse, J. Furthmuller, Efficiency of ab-initio total energy calculations for metals and semiconductors using a plane-wave basis set, *Comp Mater Sci* 6(1) (1996) 15-50.
- [16] G. Kresse, J. Furthmuller, Efficient iterative schemes for ab initio total-energy calculations using a plane-wave basis set, *Phys Rev B* 54(16) (1996) 11169-11186.
- [17] G. Kresse, D. Joubert, From ultrasoft pseudopotentials to the projector augmented-wave method, *Phys Rev B* 59(3) (1999) 1758-1775.
- [18] Y. Wang, J.P. Perdew, Correlation Hole of the Spin-Polarized Electron-Gas, with

- Exact Small-Wave-Vector and High-Density Scaling, Phys Rev B 44(24) (1991) 13298-13307.
- [19] I. Stich, R. Car, M. Parrinello, S. Baroni, Conjugate-Gradient Minimization of the Energy Functional -a New Method for Electronic-Structure Calculation, Phys Rev B 39(8) (1989) 4997-5004.
- [20] Y. Li, R.B. Thompson, Relations Between Elastic-Constants C_{ij} and Texture Parameters for Hexagonal Materials, J Appl Phys 67(5) (1990) 2663-2665.
- [21] W. Bao, X.-G. Wang, H. Ding, P. Lu, C. Zhu, G.-J. Zhang, F. Xu, High-entropy M_2AlC -MC (M= Ti, Zr, Hf, Nb, Ta) composite: Synthesis and microstructures, Scripta Mater 183 (2020) 33-38.
- [22] W. Miller, C.W. Smith, D.S. Mackenzie, K.E. Evans, Negative thermal expansion: a review, J Mater Sci 44(20) (2009) 5441-5451.
- [23] G. Hug, Electronic structures of and composition gaps among the ternary carbides Ti_2MC , Phys Rev B 74(18) (2006) 184113.
- [24] J.S. Dugdale, D.K.C. Macdonald, The Thermal Expansion of Solids, Phys Rev 89(4) (1953) 832-834.
- [25] T. Barron, R. Munn, Analysis of the thermal expansion of anisotropic solids: application to zinc, Philos Mag 15(133) (1967) 85-103.
- [26] G.W. Bentzel, M. Naguib, N.J. Lane, S.C. Vogel, V. Presser, S. Dubois, J. Lu, L. Hultman, M.W. Barsoum, E.a.N. Caspi, I. Tanaka, High-Temperature Neutron Diffraction, Raman Spectroscopy, and First-Principles Calculations of Ti_3SnC_2 and Ti_2SnC , J Am Ceram Soc 99(7) (2016) 2233-2242.

Supplementary information

Synthesis and thermal expansion of chalcogenide MAX phase Hf₂SeC

Xudong Wang^{a,b,#}, Ke Chen^{a,c,#,}, Erxiao Wu^a, Yiming Zhang^{a,c}, Haoming Ding^a,
Nianxiang Qiu^{a,c}, Yujie Song^{a,c}, Shiyu Du^{a,c}, Zhifang Chai^{a,c}, Qing Huang^{a,c,*}*

^a Engineering Laboratory of Advanced Energy Materials, Ningbo Institute of Materials Technology and Engineering, Chinese Academy of Sciences, Ningbo 315201, China.

^b School of Materials Science and Engineering, Shanghai University, Shanghai 200444, China

^c Qianwan Institute of CNiTECH, Ningbo 315336, China.

[#] These authors contributed equally to this work.

^{*} Corresponding authors.

E-mail addresses: chenke@nimte.ac.cn (Ke Chen), huangqing@nimte.ac.cn (Qing Huang).

Figures and Tables

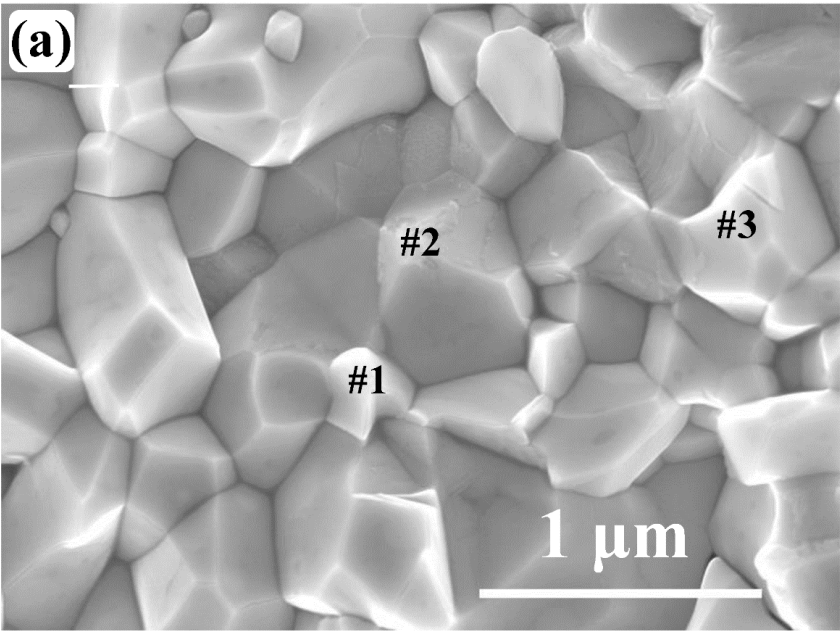


Figure S1. Fracture morphology of Hf₂SeC bulk combined with EDS point analysis.

Table S1. Elemental analysis of the selected area in **Figure S1**

Element		Hf	Se	C	O	Total
	#1	26.40	12.59	52.67	8.34	100.00
at. %	#2	31.94	16.05	49.27	2.74	100.00
	#3	28.30	13.78	56.28	1.63	99.99

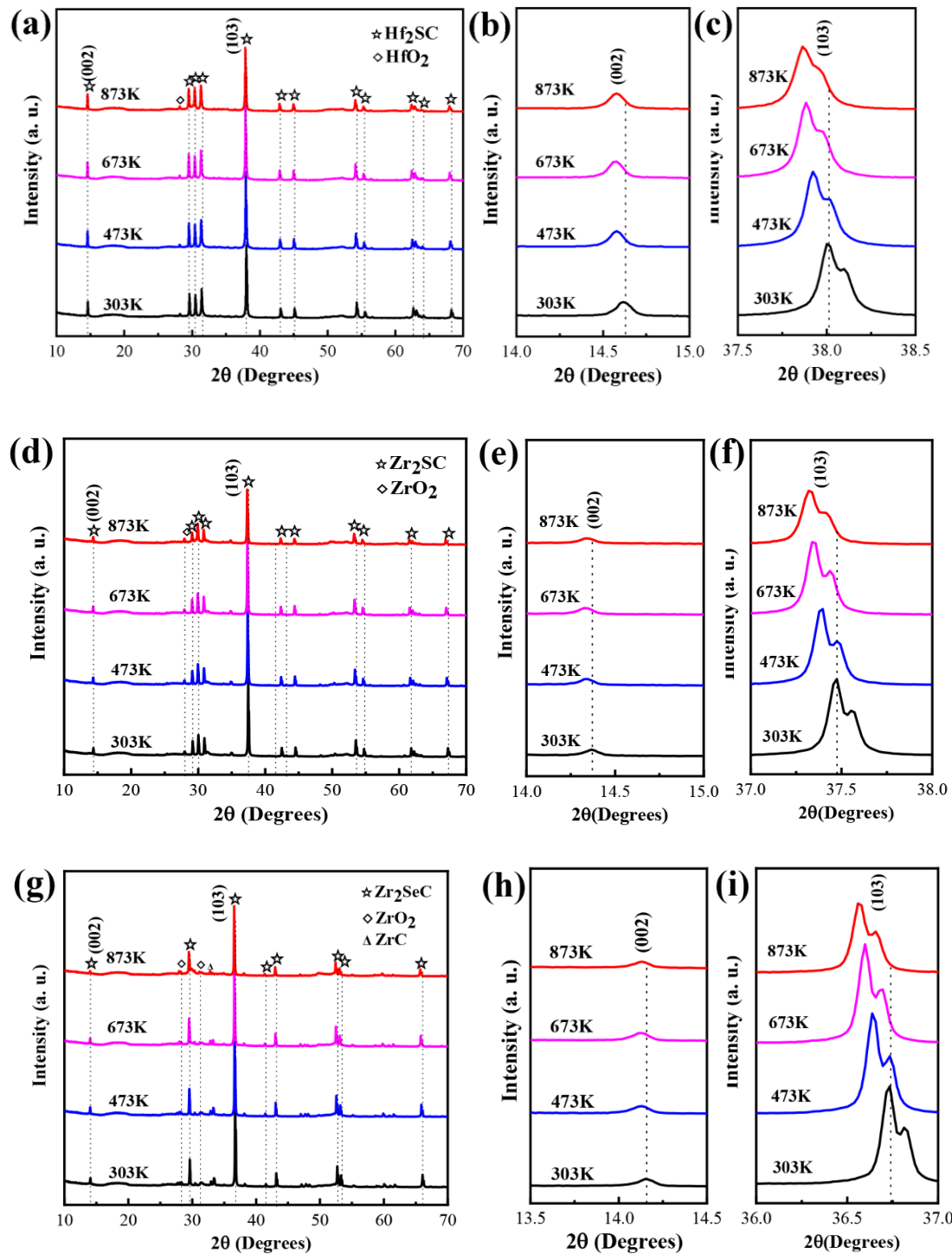


Figure S2. (a-c) High-temperature XRD patterns of Hf_2SC . (d-f) High-temperature XRD patterns of Zr_2SC . (g-i) High-temperature XRD patterns of Zr_2SeC .

Table S2. The expanded lattice parameters of four chalcogenide MAX phases using Rietveld refinements of high-temperature XRD patterns.

Compound	T (K)	a (Å)	c (Å)	R_{wp} (%)
Hf₂SeC	303	3.4204	12.3841	9.79
	473	3.4280	12.4127	10.72
	673	3.4335	12.4332	10.44
	873	3.4382	12.4523	11.01
Hf₂SC	303	3.3696	12.0143	9.48
	473	3.3761	12.0382	10.64
	673	3.3810	12.0556	10.56
	873	3.3842	12.0662	10.92
Zr₂SeC	303	3.4600	12.5145	9.83
	473	3.4689	12.5452	10.09
	673	3.4744	12.5644	10.92
	873	3.4790	12.5798	11.10
Zr₂SC	303	3.4088	12.1415	10.32
	473	3.4164	12.1671	10.76
	673	3.4218	12.1852	10.60
	873	3.4258	12.1980	10.64

Table S3. The bond length in crystal structures of Hf₂SeC, Hf₂SC, Zr₂SeC and Zr₂SC.

Compound	M-A (Å)	M-X (Å)
Hf ₂ SeC	2.774	2.305
Hf ₂ SC	2.662	2.291
Zr ₂ SeC	2.800	2.342
Zr ₂ SC	2.691	2.328